Sustainable Cities and Society 129 (2025) 106421

Contents lists available at ScienceDirect

Sustainable Cities and Society

journal homepage: www.elsevier.com/locate/scs

A mesoscopic model of vehicular emissions informed by direct measurements and mobility science☆

Ayşe Tuğba Öztürk [a], Aparimit Kasliwal [a], Helen Fitzmaurice [b], Olga Kavvada [c], Philippe Calvez [c], Ronald C. Cohen [d], Marta C. González [a,e,f,*]

[a] Department of Civil and Environmental Engineering, University of California, Berkeley, CA 94720, USA
[b] Graduate School of Education, University of California, Berkeley, CA 94720, USA
[c] ENGIE Lab CRIGEN, Computer Science and Artificial Intelligence Lab (CSAI), Paris, France
[d] Department of Chemistry, University of California, Berkeley, CA 94720, USA
[e] Energy Technologies Area, Lawrence Berkeley National Laboratory, Berkeley, CA 94720, USA
[f] Department of City and Regional Planning, University of California, Berkeley, CA 94720, USA

ARTICLE INFO

Keywords:
Urban emissions modeling
Sustainable cities
Mobile phone data
Transportation emissions
Urban mobility

ABSTRACT

Vehicle emissions pose a significant challenge for cities worldwide, yet a comprehensive analysis of the relationship between mobility metrics and vehicle emissions at scale remains elusive. We introduce the Mobile Data Emission System (MODES), a framework that integrates various sources of individual mobility data on an unprecedented scale. Our model is validated with direct measurements from a network of high-density sensors analyzed before and during the COVID-19 pandemic. MODES is used as a laboratory for scaling analysis. Informed by millions of individual trips at a metropolitan scale, we estimate the traffic CO_2 emissions with 3 accessible metrics: vehicle kilometers traveled (VKT), congestion, and fuel economy. This formulation is valuable because it is based on precise calculations reflecting variations in speed and acceleration. Across their ranges, VKT plays the greatest role in amplifying vehicular emissions up to 500%, followed by fuel economy that ranges from 20% to 300% of the average passenger vehicle. Comparatively, congestion amplifies emissions up to 50%. We confirm that cities in the Bay Area with high population density consistently show low per-person VKT. However, this density also increases congestion. Since VKT is the governing factor, urban densification reduces transportation emissions despite its impacts on congestion.

1. Introduction

Transportation is a sector that is difficult to decarbonize while it represents 29% of the greenhouse gas (GHG) emissions in the United States (U.S. Environmental Protection Agency (EPA), 2019), making it a critical barrier to achieving sustainable urban environments. Policy efforts to date have focused on improving fuel economy, alternative fuel technologies, and expanding the range of electric vehicle batteries. Despite progress in supply-side solutions, per-capita VKT and transportation CO_2 emissions have been behind reduction targets globally and are rising in most regions (California Air Resources Board, 2018; European Environment Agency, 2020; International Council on Clean Transportation, 2024). Decarbonizing passenger transportation has proven to be highly challenging compared to the other sectors (Banister, 2011; Peters et al., 2019; Shusterman et al., 2016). Recent critiques of the smart cities discourse have pointed out that while transportation systems are becoming increasingly "smarter", they are not necessarily becoming more sustainable (Yigitcanlar et al., 2019). Efficiency improvements through technology alone have not been sufficient to address deeper challenges related to emissions reduction, social equity, and unsustainable travel patterns. To effectively tackle the challenges, there is an urgent need for a comprehensive modeling framework that captures the complex relationship between mobility metrics and total vehicle emissions. Detailed analysis of these factors can inform more targeted interventions, enhance EV infrastructure, and align policies with high-emission areas contributing not only to climate change mitigation but also to healthier and more equitable cities. However, pinpointing the high-emission activities, travel demand patterns, and conditions that generate emissions remains difficult, given that emissions are distributed across travel networks.

☆ This work was supported by Engie SA, the ITS-SB1 Berkeley Statewide Transportation Research Program and the California Air Resources Board, United States.

* Corresponding author at: Department of Civil and Environmental Engineering, University of California, Berkeley, CA 94720, USA.
E-mail address: martag@berkeley.edu (M.C. González).

https://doi.org/10.1016/j.scs.2025.106421
Received 24 December 2024; Received in revised form 29 April 2025; Accepted 30 April 2025
Available online 27 May 2025

To address diverse evaluation needs, urban transportation emissions modeling uses three main approaches: physics-based, empirical, and data-driven models. Physics-based models, centered on vehicle specific power (VSP), measure power demand on vehicles, accounting for forces like aerodynamic drag, rolling resistance, acceleration, and incline (Faris, Rakha, Kafafy, Idres, & Elmoselhy, 2011; Fontes, Pereira, Fernandes, Bandeira, & Coelho, 2015). These models integrate three key components: travel demand models, which estimate origin–destination flows using travel surveys, highway counts, fuel sales, and land-use data (Bandeira, Coelho, Sá, Tavares, & Borrego, 2011), and traffic simulators, which simulate vehicle flow, route choices, and speed patterns based on calibrated road network parameters (e.g., road types, traffic lights) (Anya, Rouphail, Frey, & Schroeder, 2014). These inputs are crucial for emission simulators, which calculate total travel emissions in each VSP mode.

While the final step of physics-based models is robust and relies on Newton's laws of motion, significant uncertainty exists in travel demand and traffic simulation phases. These components require complex software prone to errors in calibration and data handling, often leading to discrepancies in emissions estimates (Abou-Senna, Radwan, Westerlund, & Cooper, 2013; Anya et al., 2014). As a result, most validated models estimate emissions primarily at the link level, with some extending to broader urban areas. These models excel in link-level analysis, guiding vehicle and road network design (Fontes et al., 2015) and modeling external traffic losses (Patankar, Lin, & Patankar, 2021). However, they lack accuracy at larger spatial scales, where data requirements and calibration challenges hinder precision. Calibration errors can reach up to 16% (Anya et al., 2014), and broader inventories underestimate emissions by up to 28.1% (Gurney et al., 2021).

Empirical models, or direct measurement models, use sensing technologies like traffic sensors, primarily deployed on highways (Kwon, Varaiya, & Skabardonis, 2003; McDonald, McBride, Martin, & Harley, 2014; Wu et al., 2022) and less frequently in city centers (Zhang et al., 2018). These sensors provide data on vehicle counts, types, and speeds, which is combined with speed-dependent emission factors to estimate emissions at zonal and link levels. Additionally, onboard vehicle devices create regression-based models (Oehlerking, 2011). Dense CO_2 sensor networks, combined with Bayesian inversion, attribute emissions to specific source activities like transportation and home heating (Caubel, Cados, Preble, & Kirchstetter, 2019; Gurney et al., 2009). While monitoring methods are crucial in constructing and validating data-driven emission inventories, there are two shortcomings that call for individual mobility estimates. First, sensors are expensive to deploy and maintain over large regions to directly inform city inventories. Second, sensor-based estimates are not capable of attributing emissions to the origin and destinations associated with the travel activity. The latter is particularly important for transportation planning authorities for measuring carbon emissions by source activity at urban scale to achieve decarbonization goals (Ramaswami et al., 2021).

Data-driven models, more user-friendly and accessible than physics-based or empirical models, integrate multiple data sources on travel demand and road conditions. These methods can be further divided into three groups based on the mobility data being used: (a) local traffic volumes (Gately, Hutyra, & Wing, 2015; Gurney et al., 2012), (b) aggregated origin–destination (OD) flows (Gately, Hutyra, Peterson, & Sue Wing, 2017), and (c) individual mobility data (Blaudin de Thé, Carantino, & Lafourcade, 2020; Böhm, Nanni, & Pappalardo, 2022; Miller & Ibrahim, 1998; Nyhan et al., 2016). To understand the difference between these three approaches, we need to differentiate the outputs of these models as *local emission estimates* and *emission production estimates*. Local estimates quantify emissions within a region, route, or road segment. Methods using local traffic volumes estimate the emissions in the place where they occur. While these models provide accurate estimates locally, they lack information regarding the traveler, source, and destination of the trip. This information holds significant importance for policy-making and demographic analysis. The emission simulation tools used by planning agencies in EU (Ntziachristos, Gkatzoflias, Kouridis, & Samaras, 2009) and US (California Air Resources Board, 2017; United States Environmental Protection Agency (USEPA), 2023) also fall into the *local emission estimates* category. They report values over regions given the input VKT, speed and vehicle type distributions. Performing both road level and individual level analysis are possible, yet it can take months to customize and run the models. Furthermore, the current models are not generalizable to regions other than their context. *Emission production estimates* quantify CO_2 emitted across the travel network by the origin of the individual travelers and link them to their locations of residence. This type of quantification is possible with individual mobility data or OD flows. Individual mobility estimates have been developed using acceleration, speeds, and car model (Oehlerking, 2011; Panis, Broekx, & Liu, 2006; Smit, Ntziachristos, & Boulter, 2010). We refer them as microscopic, and our goal is to develop a mesoscopic model that estimates CO_2 emissions with quantities related to the drivers such as percentage of congestion, distance of travel and fuel economy of the vehicle used.

Individual mobility data from mobile phones have been used in various applications (Pappalardo, Manley, Sekara, & Alessandretti, 2023). For example, studies on multiple cites have uncovered scaling laws relating population to distribution of facilities and socioeconomic activities at macroscopic scale (Barthelemy, 2019a; Bettencourt, 2013; Bettencourt, Lobo, Helbing, Kühnert, & West, 2007; Depersin & Barthelemy, 2018; Newman, 2005; Xu, Olmos, Abbar, & González, 2020). Universal laws govern the collapse of traffic networks (Olmos, Çolak, Shafiei, Saberi, & González, 2018) or traffic management strategies via smart phone applications (Çolak, Lima, & González, 2016). A growing body of literature, including recent reviews (Milojevic-Dupont & Creutzig, 2020), highlights the potential of combining mobility data with machine learning to move beyond generic mitigation strategies towards scalable, spatially differentiated climate solutions. Our task at hand is to leverage this emerging toolkit of mobility science to inform urban sustainability strategies.

This work utilizes mobility science methods in the analysis of passenger vehicle emission estimates. With this in mind, we present MODES, a portable framework to estimate vehicle emissions using various individual data sources. To that end, we integrate, at unprecedented scale, call detail records (CDR's) for the Bay Area (Xu, Çolak, Kara, Moura, & González, 2018), aggregated Location Based Service (LBS) data from SafeGraph (2021) and Uber Movement Speeds data (Uber Movement, 2021).

To validate our model, we utilize data from both before and after the COVID-19 shelter-in-place (SIP) orders in the San Francisco Bay Area. SIP orders significantly altered individuals' travel behavior, making it an ideal opportunity to assess our model's performance under different conditions. Therefore we performed estimates for these two periods separately. We estimate the travel behavior and the road congestion for six weeks before and after the SIP orders, implemented on March 16th 2020. We combine the traffic estimates with the StreetSmart fuel consumption model (Kalila, Awwad, Di Clemente, & González, 2018; Oehlerking, 2011) and convert these values to tail-pipe CO_2 emissions. We compare our estimates with direct CO_2 sensor measurements and a hybrid model of highway vehicle counts and emission factors.

To our knowledge, this is the first study that utilizes individual mobility extracted from mobile phones in data-driven emissions estimates at the mesoscopic scale. This allows us to link CO_2 emissions to the home locations of travelers. We further investigate the interplay of population density and road network structure on individual travel demand and their associated emissions. Confirming that cities with high population density are characterized by low per-person VKT, low per-person CO_2 emissions, and high congestion levels. Yet, based on our observations and the ranges of the trip variables (VKT, percentage of congestion, and fuel economy) VKT has the strongest effects on emissions.

We analyze individual trips at varying percentages of congestion, to uncover a bottom-up law that incorporates VKT, congestion, and fuel economy to estimate emissions from millions of individual trips. The parameters we utilize are not specific to a particular study region, allowing our analysis to be applicable to trips in any city given the data availability. Current scaling laws depend on top down estimates of the form $tCO_2 \sim N^{\beta}$, where N is the population size and its emission production in tons (tCO_2) (Louf & Barthelemy, 2014b). Our approach is an advancement over the existing scaling laws by incorporating parameters directly affecting vehicular emissions. Since these parameters are not context or city specific we also maintain the scalability and modularity of the findings.

A critical step is the validation of our estimates. Existing data-driven emission estimation frameworks are validated with other data-driven emission inventories. These inventories often have similar underlying assumptions. In contrast, to validate and test the robustness of MODES, we used completely independent measurements from the Berkeley Air Quality and CO_2 Network ($BEACO_2N$). We performed a comprehensive validation and calculated statistics in regions with different characteristics (i.e. highway length, residential road length) and resolutions (i.e. from 1 to 25 km^2 spatial resolution, averaging from 1 to 5 measurement days). We validated the results from before and COVID-19 separately ensuring accuracy under different demand levels. We found that at a spatial resolution of 9 km^2 and 5 days of measurement, the median difference between MODES and $BEACO_2N$ is 32%. This is advancement over the major inventories in use, that may differ more than 100% at lower spatial resolutions (Gately & Hutyra, 2017).

The main contributions of our work include:

(1) We establish a scaling law that quantifies the relationship between emissions, VKT, congestion, and fuel economy, utilizing easily available metrics in diverse urban contexts. This approach greatly simplifies the estimation of emissions.
(2) Scaling analysis confirms VKT as the primary parameter influencing emissions. Building upon this foundational finding, our analysis quantifies the relative influence of VKT alongside congestion and fuel economy. This enhances our understanding of the complex dynamics influencing vehicular emissions in urban systems.
(3) MODES represents a significant advancement over local emission estimates by quantifying emissions at the individual traveler level. This capability allows MODES to directly inform sustainable urban planning regarding vehicle electrification, equity in air pollution exposure, and land use planning.
(4) Unlike other models that lack validation or are validated across large metropolitan regions, MODES stands out by being validated through direct measurements of CO2 emissions at various spatial resolutions.
(5) MODES is the first study utilizing a travel model informed by passively collected mobile phone activity data in emissions estimates.

This paper is organized as follows. The Introduction provides the background, motivation, literature review, and our positioning within the emissions modeling landscape. Section 2 presents the main results of the study. Section 3 discusses the broader implications of the findings, including policy relevance and sustainability framing. Section 4 outlines directions for future work, while Section 5 concludes. Finally, Section 6 details the data sources, methodological steps, and validation procedures. We placed the Methods section at the end to maintain a logical narrative flow and to highlight the study's key insights early.

2. Results

2.1. Congestion estimates and travel behavior

We characterize the typical weekday travel behavior before and during the shelter in place (SIP) orders in the Bay Area road network. All Bay Area counties imposed SIP orders starting on March 16th, 2020. We defined the before SIP period as six weeks until this date and during SIP period as six weeks following this date. The primary purpose of utilizing the post-COVID-19 period is to conduct a comprehensive validation process.

The travel demand used in this work is based on the urban mobility model TimeGeo, a simulation of individual mobility using CDRs (Jiang et al., 2016). The individual mobility patterns of the simulated users are shown to align well with the 2010–2012 California Household Travel Survey (CHTS) and the 2009 National Household Travel Survey (NHTS) (Xu et al., 2018). Travel surveys, while valid, are costly methods of data collection that only capture a limited portion of the population and may not encompass all individual trips undertaken. TimeGeo presents a comprehensive and valid estimate of the individual travel demand. This model represents the typical weekday travel behavior for the before SIP period. To extend this model to each day of the week for before and during SIP periods, we used SafeGraph data. We multiply the hourly travel demand between each origin and destination pair with a scaling coefficient retrieved from SafeGraph (see Supplementary Notes S2). To use the resulting travel demand for vehicles, the standard is to estimate vehicle trips from the total trips by scaling total trips with the vehicle usage rate of the home census tract (see Supplementary Notes S3). The resulting vehicle demand is 9.6 million vehicle trips out of 13 million passenger trips within the Bay Area for a typical weekday. The hourly and weekly distribution of the weekday trips for before and during SIP is shown in Fig. 1A. We find that due to the SIP orders the total number of trips decreased by 52% and 59% during the morning peak. In Fig. 1B, we show the number of trips between each origin and destination pair grouped by the distance. The variations in number of trips are due to the differences in travel demand during different times of the day. Interestingly, while the number of trips decreased in total, there was an increase in the share of trips above 150 km. The total VKT decreased by 44% from 234M km/day to 131M km/day. The comparison of these findings are consistent with the report of the Bureau of Transportation statistics COVID-19 travel behavior changes (Bureau of Transportation Statistics, 2022).

We perform road network analysis within a bounding box formed by the locations of mobile phone users. We modeled the San Francisco Bay Area road network as a weighted, directed graph where edges represent the road segments and the edge weights are the speeds, travel times and road lengths. Road geometries are retrieved from Open Street Map (OSM) and corresponding hourly speeds are provided by the Uber Movement Speeds API. Travel time on each edge is calculated using the road geometries and hourly speed values. We identified the free-flow speed as the 85th percentile of all speed values observed on a road segment during a week. Then the congestion level in a region is defined as the percentage change in the travel time in comparison with the free-flow travel time. Most of network-wide congestion occurs at 5 PM before the SIP orders and ranges between 30 and 37% depending on the day of the week. During the SIP orders, the 5PM's network-wide congestion dropped to 14 to 19%. The study region and the congestion level per road segment is illustrated in Fig. 1C and D.

2.2. Fuel economy variations in traffic

In this work, we employed the StreetSmart (Oehlerking, 2011) model to estimate each trip's fuel consumption. This model requires the speed profiles on the road segments and accounts for the vehicle efficiency variations under different speed and acceleration levels. The model requires four variables as shown in Eq. (1).

$$FC_{gal} = k_1 T_{idle} + k_2 T_{move} + k_3 \int_x |a| dx + k_4 L \tag{1}$$

The first term accounts for the idling energy consumption; the second term accounts for the energy depending on the time of the

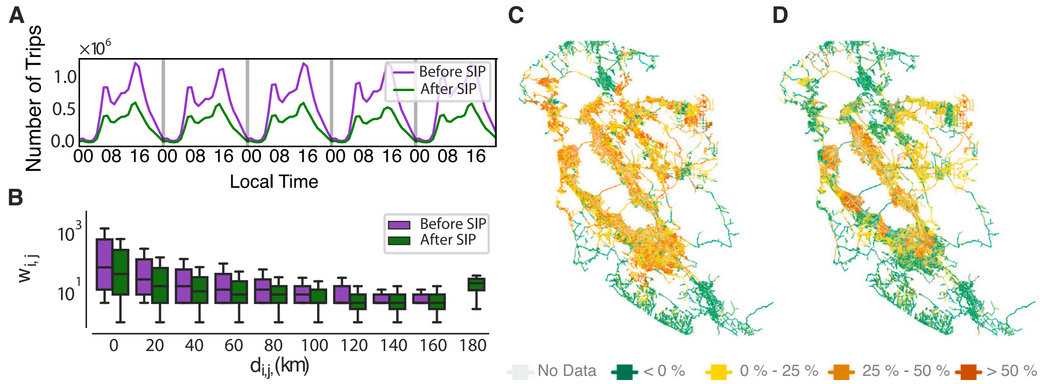

Fig. 1. Travel demand and congestion levels before and during shelter-in-place orders. Congestion level is defined as percentage change in travel time compared to the free-flow travel time. Congestion levels are calculated using hourly average speeds for each road segment in the network. (A) Weekday travel demand extracted from CDR and LBS data, aggregated hourly. (B) Travel demand between i (origin) and j (destination) grouped by Haversine distance. Congestion level in the road network on Monday 5PM before shelter-in-place orders (C) and during shelter-in-place orders (D). Base map OpenStreetMap contributors.

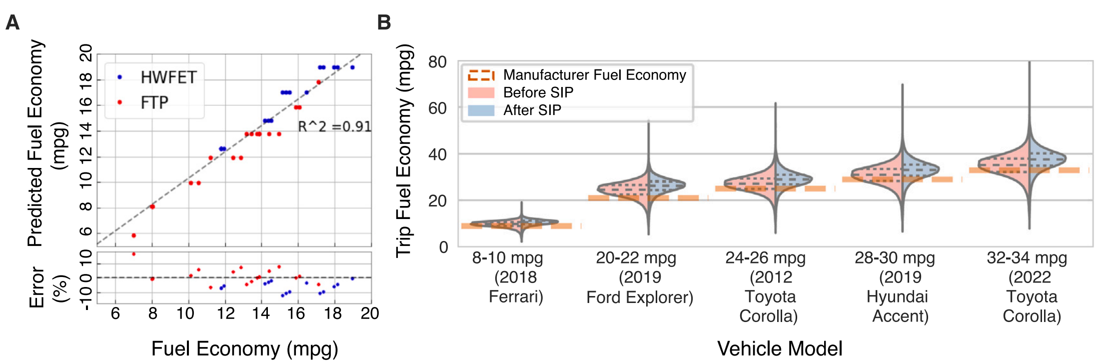

Fig. 2. Vehicle fuel consumption model (A) Validation of the StreetSmart fuel economy estimates with Autonomie vehicle fuel consumption simulations. The fuel economy estimations use EPA's FTP-75 (urban) and HWFET (highway) standard speed profiles. (B) Variations in on-road fuel economy by manufacturers reported fuel economy in the same analysis period. The differences between the actual fuel economy and the manufacturers' value can be as high as 70%, as shown in the distributions, illustrating the impact of the road network traffic. Due to a decrease in congestion, before SIP's order trips have a 6%–7% lower median fuel economy than the during SIP order.

movement; the third term accounts for the acceleration and deceleration over a given distance, and the final term accounts for the energy use for the distance traveled. The k's in the model are vehicle efficiency-specific multipliers. The model has over 96% accuracy in tests performed with vehicles GPS coordinates and output fuel consumption values read from on board diagnostics (OBD-II) devices. To use this model for any vehicle in the Bay Area fleet, we calibrated the vehicle efficiency constants and further validated the calibrated model. For calibration of the constants *k*s, we used fuel efficiency values provided by the Environmental Protection Agency's (EPA) 2021 report (U.S. Department of Energy, 2021) and FTP-75 speed profiles used in EPAs urban fuel economy testing procedure ((EPA), 2021). (see Supplementary Notes S4 for a list of calibrated coefficients). We validate our calibration by comparing them with the results of the software Autonomie, a fuel consumption simulator developed by the Argonne National Laboratory (Yao & Moawad, 2019). We tested the model for five vehicles in the software under EPA's FTP-75 and HTP-75 drive cycles (see Supplementary Note S4). We recorded the mean absolute error of all tests, obtaining 5% on average, as shown in Fig. 2A.

To use this model to estimate city-wide fuel consumption, we assigned each vehicle trip a route on the network, based on the edges with the shortest travel time. Each trip's travel time, speed, and distance is calculated from the edge weights. The idling time is imputed only if a stop sign, traffic light, or crossing is present at the nodes traversed. The acceleration variable in the model is approximated since we do not have high-resolution speeds along the edges. We use constant speeds along the roads as extracted from the Uber Movement Speeds. We then included the acceleration/deceleration if a stop or a speed change between edges is present (for details see Supplementary Notes S5). For example, on an average Monday, we have 9.6 million daily trips before SIP orders and 4.2 million distinct origin and destination pairs. We assigned 5.3 million distinct routes and recorded associated speed profiles.

The fuel consumption of all the routes are calculated for different manufacturer-reported fuel economies with the calibrated StreetSmart model. Due to traffic conditions, the average of our estimated fuel efficiency of the vehicles varies from the manufacturer-reported fuel economy by 17%, and the differences in the actual fuel economy of the same car can be as high as 70% as it is shown in the distributions of Fig. 2B. These variations illustrate the impact of the road network traffic on the actual vehicle efficiency. We observe that trips before the SIP orders have a 6%–7% lower median fuel efficiency than the trips during the SIP orders. The difference arises from the less congested states of the roads.

2.3. Emissions comparisons with sensor-based estimates

In urban areas, disagreement between on-road emission inventories can be as large as 40%–100% (Gately & Hutyra, 2017). The uncertainty arises from the model assumptions and differences in underlying data sources such as vehicle efficiency, emission factors, magnitude and spatial distribution of VKT, and travel speeds. In MODES, emissions are calculated only for the personal vehicles for an average Bay Area

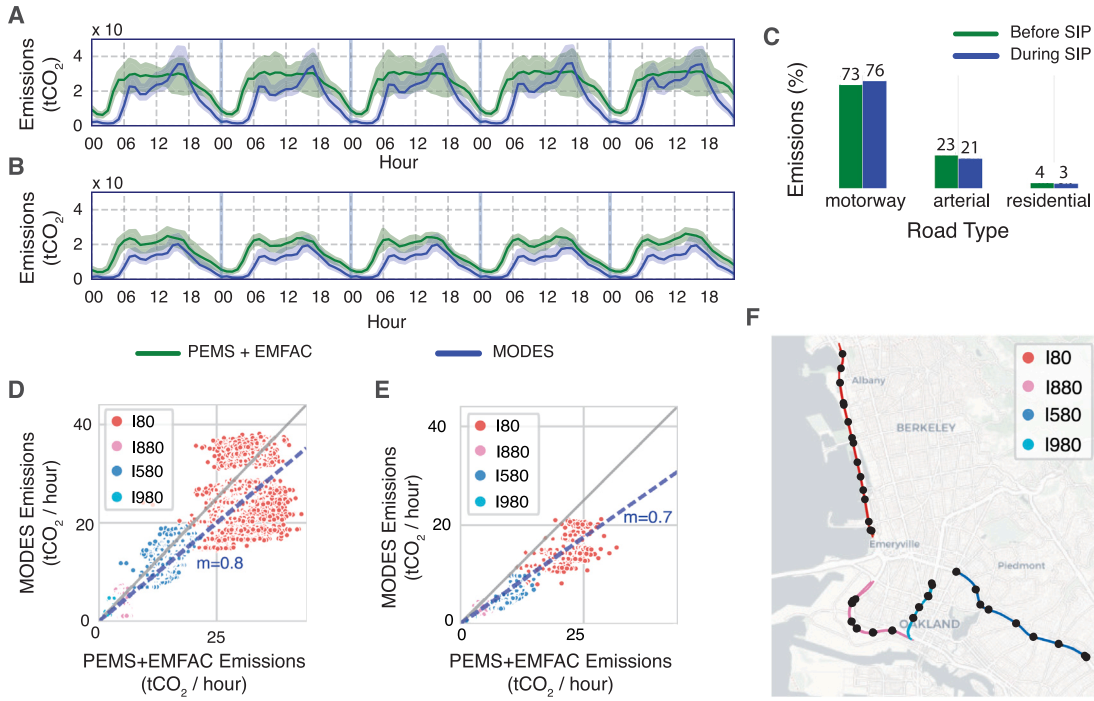

Fig. 3. On-road vehicle emissions validation. Comparison of PEMS + EMFAC estimates and MODES on I-80 highway for (A) an average weekday before the SIP order and (B) for an average weekday during the SIP period. (C) Percentage of total emission estimates for each road class before and after SIP estimated by MODES. Highways have the largest share of emissions both before and after SIP. (D) Comparison of hourly PEMS + EMFAC and MODES emission estimates on 4 highway segments before SIP. The best-fit line $y = 0.8x$ (blue) and $y = x$ (gray) are shown. (E) Comparison of hourly PEMS + EMFAC and MODES emission estimates on 4 highway segments after SIP. The best-fit line $y = 0.7x$ (blue) and $y = x$ (gray) are shown. (F) Highway segments used in part D. Base map OpenStreetMap contributors.

vehicle with 25 mpg efficiency (Fitzmaurice et al., 2022). Trucks fuel consumption is not included due to a lack of data on heavy-duty vehicles' temporal and spatial distribution. In order to get emissions, fuel consumption estimates for the personal vehicles are then converted to CO_2 emissions assuming 8887 [g CO_2] is emitted per gallon of fuel burned (U.S. Environmental Protection Agency (EPA), 2018) (See Supplementary Notes S8).

We compared our resulting emission estimates with the direct measurement of the Berkeley Air Quality and CO_2 Network ($BEACO_2N$) and also with the Emissions Factor model (EMFAC2017) of the California Air Resources Board (CARB) (California Air Resources Board, 2017) applied to vehicle flows acquired from CalTrans Performance Measurement System (PeMS) (Caltrans Performance Measurement System, 2021). After COVID-19 SIP estimates are mainly used for validation purposes, making the results robust to different travel demand levels within the network.

The EMFAC2017 model provides emissions factors for each vehicle class and speed level. However, getting the aggregate emissions for road segments requires further knowledge of vehicle counts and speeds. We followed the method presented in Fitzmaurice et al. (2022) and combined the emissions factors with the vehicle count, truck percentage, and speed data obtained from PeMS. The PeMS data is only available for highways. Therefore, we first validated our results only on highways which account for 73% and 76% of all vehicle emissions before and during the SIP. Selected highway segments; I580 I80, I880 and I980 are presented in Fig. 3. These segments were selected due to the differences in length and average truck percentages. We observe that our estimates are within 35% of the PeMS-EMFAC2017 model for daytime emissions between 7 am and 9 pm. Before and during SIP emission comparisons for a typical weekday for a 5 km stretch of the I80 are presented in Fig. 3A–B. Emissions comparisons for the rest of the highways are provided in the Supplementary Figure S9.

To evaluate the performance of MODES in non-highway emissions, we compared the results with the $BEACO_2N$ estimates. Comparison of data-driven models with the direct emissions estimates is expected to have differences as there are uncertainties involved in both processes. The CO_2 concentration measurements are recorded by a $BEACO_2N$'s dense network of sensors and attributed to a source using a Bayesian inversion method (Turner, Kim et al., 2020). We performed analysis on transportation emissions in the 40% CO_2 influence region (Fitzmaurice et al., 2022), shown inFig. 4(D–F). Percentage difference is calculated as $\frac{(CO_2^{BeaCO_2N} - CO_2^{MODES})}{CO_2^{BeaCO_2N}}$.

Hourly airflow models at high spatial resolution can vary significantly due to uncertainty in wind speed and direction (Lauvaux et al., 2016). In order to find a good validation resolution, we tested the difference between $BEACO_2N$ and MODES estimates at varying aggregation levels and highway lengths. Results are shown in Fig. 4. We first aggregated the transportation emissions zones from 1 to 25 km^2 areas to account for the possible errors in the airflow direction model. Spatial aggregation significantly decreased the range and median of the difference between the two models up to 9 km^2. We further aggregated the results temporally for 9 km^2 cells. We take the average of the weekdays available for each measurement hour based on the sensor measurements. Temporal aggregation further reduced the range and median of the difference. Finally, we found that MODES underpredict regions with fewer highways.

The spatial variation of the emissions for the average 3 PM travel behavior before and after the SIP is illustrated in Fig. 4D–G. The results shown are for 9 km^2 cells and aggregated temporally as described above. The cells are colored based on the quantile breaks of each model and measurement period. When we compare Fig. 4D and E, MODES and $BEACO_2N$ have a similar spatial distribution of the emissions. MODES generally underpredict. The underprediction of MODES is expected since we do not account for heavy-duty vehicles (HDV) in our analysis. Our high prediction in highways could be due to the high flow values assigned to the highways in the vehicle assignment method. When we compare Fig. 4D and F, and Figs. E and G, we observe that the model captured the decrease in emissions during the SIP order.

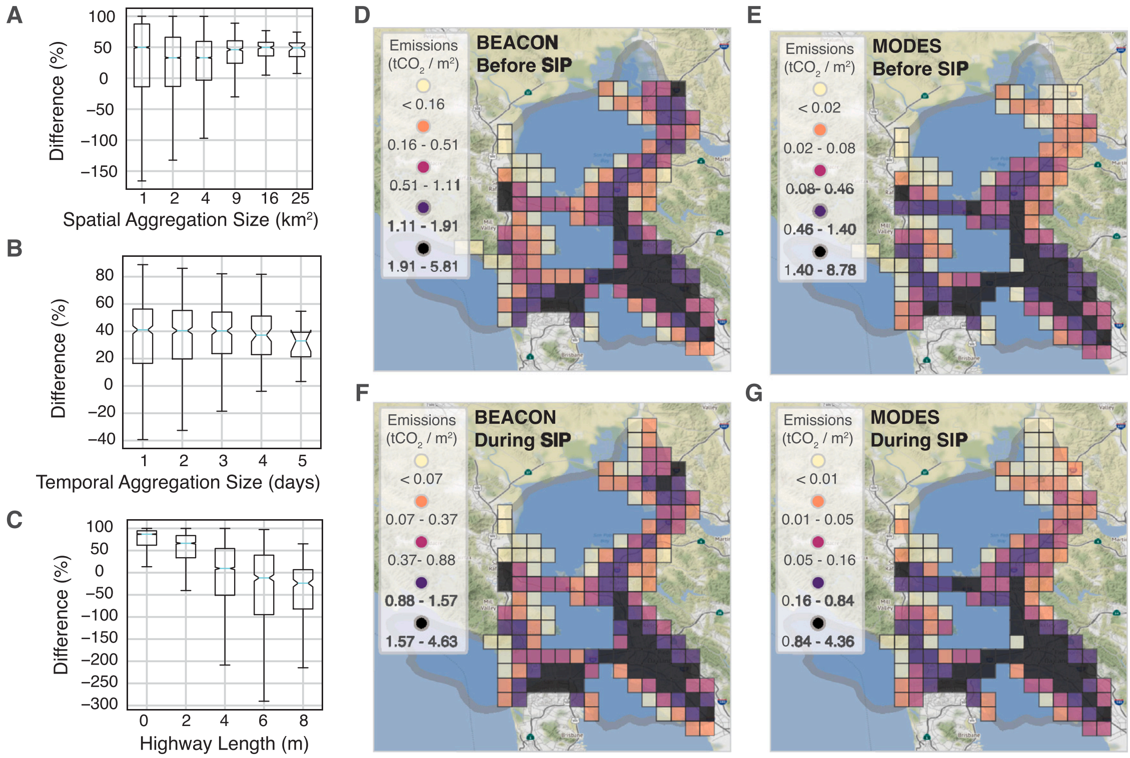

Fig. 4. Comparison of MODES CO_2 emissions estimates with $BeaCO_2N$ measurements. (A) Comparison under different spatial aggregation units. (B) Comparison under different temporal aggregation units. The difference between $BeaCO_2N$ minus MODES is calculated for 9 km^2 grids. (C) Comparison in cells with different highway lengths. As the highway span increases, our estimates overpredict. (D–G) Local emission estimates within the $BEACO_2N$ domain (Gray line indicates the region that contains the largest 40% of the total network influence). Emissions are spatially aggregated into 9 km^2 cells and temporally aggregated within the 6 weeks before and after the SIP analysis period. Quantile breaks are adopted to demonstrate the spatial distribution of emission hot spots. (For interpretation of the references to color in this figure legend, the reader is referred to the web version of this article.)

Mesoscopic model of vehicular emissions

This section investigates the relationship between vehicular emissions and urban metrics. We analyze the role of urban form and travel patterns. Scaling laws in urban systems have been studied widely in various domains. Response of the quantity Y to a change in the independent variable, X, is represented in the form of a power law:

$$Y = \alpha X^{\beta} \tag{2}$$

Data from cities present scalings of the form of Eq. (2) where X is population and Y various socio-economic indicators (Bettencourt, 2013; Bettencourt et al., 2007; Bettencourt, Samaniego, & Youn, 2014). In the urban domain, scaling of emissions over a region with its population size has attracted significant attention (Fragkias, Lobo, Strumsky, & Seto, 2013; Mohajeri, Gudmundsson, & French, 2015). Yet no consensus has been reached on the relationship. The value of the exponent β differs for the same data set with different urban borders (Arcaute et al., 2015; Cottineau, Hatna, Arcaute, & Batty, 2017; Louf & Barthelemy, 2014b). The presence of noise and lack of enough orders of magnitude on axes can pose a problem in establishing a significant scaling relationship (Barthelemy, 2019b).

Street length, congestion, and VKT are other scaling relationships explored (Louf & Barthelemy, 2014a; Mohajeri et al., 2015). Yet these existing studies lack reliable emission estimates or the resolution of the data is too low to establish a relationship with trips over the road networks.

We investigate scaling relationships between the daily emissions (gCO_2/day) production within the network in relation to VKT and population. The daily emissions are calculated based on the home locations and the trips extracted from the TimeGeo model (Xu et al., 2018). CO_2 emission production by travelers across the Bay Area are aggregated into the home cities as defined by the US Census Bureau. There are 162 cities in the analysis region. The CO_2 emission production calculations were made based on an average vehicle efficiency of 25 mpg in the Bay Area.

To calculate the local scaling exponent, we generated scaling tomography plots suggested by Barthelemy et al. for noisy data (Barthelemy, 2019b) (see Supplementary Figure 5A). This method allows us to identify threshold effects and multiple scaling exponents that are not detectable by classical least squares fitting. A super-linear scaling with $\beta_{eff} = 1.12 \pm 0.13$ is found between the city population and the CO_2 emissions produced by them as shown in Fig. 5C.

As shown in Fig. 5D, we find a linear relationship between the total VKT and the total CO_2 emissions produced by the city residents. We observe a clear linear relationship and no threshold effect in the tomography plots (see Supplementary Figure 5B). The slope of the best-fit line is the emission efficiency (gCO_2/km) of a trip and it varies among different cities. We find 209 gCO_2/km as the mean emission efficiency of the cities in our domain and the value can range between 175 to 225 gCO_2/km. The difference between the cities arises from the different congestion levels experienced and the stop and go traffic.

We also analyze the population density as a function of $VKT/person$. Cities cluster into four groups within the Bay Area travel network in the analysis region, as shown in Fig. 5A–B using K-means clustering. We observe that high population density is associated with low VKT per person, but in low population density zones, VKT per person varies. Also, high population density results in high congestion levels experienced by their residents (see Supplementary Figure 6). In cluster 2 in Fig. 5A–B, we can observe that low population density cities are uniquely characterized by a lower VKT/person. Yet, when we extend the analysis from individual cities to metropolitan-level interactions, we see that a dense urban core can drive longer commutes for residents of peripheral cities. This core–periphery dynamic is likely

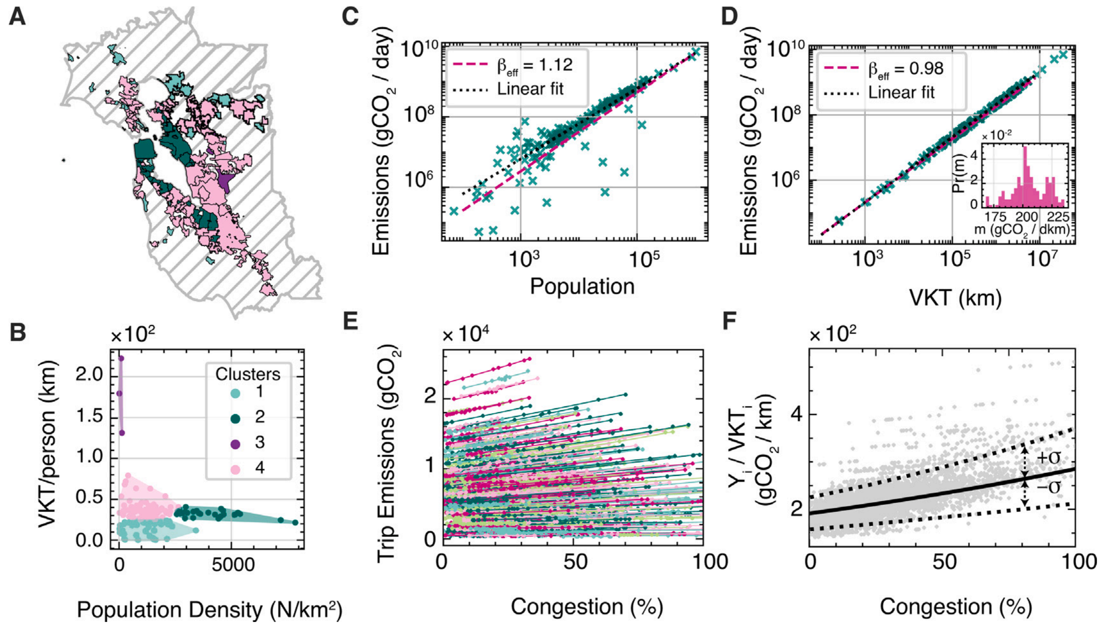

Fig. 5. Scaling of on-road vehicle emissions (A–B) 162 Cities in the analysis region are clustered into four groups (different colors) based on population density and per-person VKT within the travel network. In cluster 2, we can observe that low VKT/person uniquely characterizes high population density. (C) The power-law relationship between the local population and the network-level vehicle emissions produced in the Bay Area. A super-linear scaling with $\beta_{eff} = 1.12 \pm 0.13$ is found. (D) The linear relationship between the total VKT by the city residents and total emissions produced by them. The inline plot shows the distribution of the slope ($g\mathrm{CO_2/km}$) per city, and the median is at 209 $g\mathrm{CO_2/km}$. (E) Emissions of trips at the different congestion levels, keeping everything else (stop time, acceleration, distance) constant. Each line is Eq. (3) (F) Emissions per trip by the law presented in Eq. (4) with a vehicle efficiency of 25 mpg (10.6 km/l). The region within the dotted lines is the one standard deviation confidence interval. (For interpretation of the references to color in this figure legend, the reader is referred to the web version of this article.)

to be the reason for cities belonging to cluster 3 and 4 to have higher VKT/person.

To quantify the impact of congestion and VKT, we further check emissions at the trip level for the same route at varying congestion levels. Fig. 5E illustrates 1500 trips where each dot represents the trip's emissions for a given congestion level. The best fit of gCO_2 emissions (Y_i) of trip i is

$$Y_i = \alpha_i \exp(\beta_c X) \tag{3}$$

with $\beta_c = 0.004 \pm 0.001$ for all trips. At the same congestion level, emissions for a trip can vary significantly due to the VKT. The route difference presents itself in the intercept α_i, of each trip's emissions best-fit line. The α_i is, in turn, a function of the VKT and the fuel economy (FE). For trips with a 25 mpg vehicle, $\alpha_i = \gamma VKT_i$, and $\gamma = 190.6 \pm 33.3[g\mathrm{CO_2/km}]$

Fig. 5F shows Eq. (3) divided by VKT_i, where 89.7% of the trips lie within the confidence interval. The trips outside this region are short in distance and have much longer idling times per VKT. Supplementary Figure 8 illustrates the distribution of VKT, idle time per VKT, and acceleration per VKT for the trips outside and inside the confidence interval. We show that the trips outside the confidence interval have a mean idling time per VKT of 60 s, whereas this value is 18 s for the rest of the trips.

This relationship can be generalized to any fuel economy when we write α_i as a function of the manufacturer's reported fuel economy of the vehicle. Fitting procedure is described in Supplementary Notes 7. Supplementary Figure 9 illustrates that the best fit for this relation is $\gamma = 2006.53 \pm 314.32[g\mathrm{CO_2/l}]/FE$ where FE stands for the fuel economy in [km/l]. We get the general expression per trip emissions:

$$Y_i = \frac{2006.53[g\mathrm{CO_2/l}]}{FE[\mathrm{km/l}]} VKT_i \exp^{0.004X} \tag{4}$$

The median vehicle travel distance in the Bay Area is 15 km, and 95% of the trips are below 70 km. This means VKT can vary emissions by 10% to 500%. Vehicle efficiency approximately ranges between 10 mpg to 119 mpge (mpg equivalent for electric vehicles), that would change the estimates of Eq. (4) from 20% to 300% of the mean efficiency for a passenger combustion vehicle. Varying the congestion level from free-flow to 100% can increase the emissions by 1.5 times or 50%. However, 100% congestion is rarely experienced, 95% of the trips in the Bay Area experience congestion levels below 62% which corresponds up to 28% enhancement of vehicular emissions.

Eq. (4) is derived at the individual trip level, independent of specific city characteristics. While the above analysis is conducted for the Bay Area travel network, the equation can be reproduced for any city. To validate its reproducibility, we tested the MODES law using emissions data generated through the Simulation of Urban Mobility (SUMO) software in Boston, Los Angeles, and Rio de Janeiro. These reproducibility tests demonstrated that 13–15% of the trips fall within the defined confidence level, confirming the robustness of the MODES law across diverse urban environments. Supplementary Fig. S10 provides visual comparisons, and further details of the evaluation process are outlined in Supplementary Notes S9. Despite relying on three simplified metrics—VKT, congestion, and fuel economy—the MODES law aligns closely with the simulated emissions, supporting its generalizability.

The availability of VKT, congestion, and efficiency parameters enables this equation to provide a robust and straightforward estimation of transportation emissions with high spatial and temporal granularity. The MODES framework can be replicated to conduct in-depth analyses and reveal location-specific emission trends. The mobile phone activity data used in MODES is readily available in modern cities, and average road speeds are obtained through the Uber Movement Speeds API. While we rely on average speed data, which is more readily available than instantaneous speed values, our validation process confirms the robustness of the results.

3. Discussion

3.1. Key findings and interpretation

This study introduces MODES, a data-driven framework for estimating vehicle emissions based on individual mobility data extracted from mobile phones. We quantify the relationship between vehicular emissions, congestion, and VKT with a simple and scalable equation. The key advantage of this formulation lies in the accessibility of its inputs. Congestion levels are available through datasets such as TomTom Traffic Index, VKT can be estimated from fuel sales, traffic sensors, or travel surveys, and fleet fuel economy is often available from vehicle registration databases. Using this equation, we found that VKT is the dominant factor influencing aggregate emissions, far outweighing the effects of congestion. While there is no clear linear relationship between population density and emissions, our clustering analysis reveals that high-density cities tend to produce lower per capita emissions, largely due to shorter travel distances—even though they experience higher congestion levels. In contrast, low-density, peripheral cities often show higher emissions per capita as a result of longer VKT.

Reproducibility of the MODES results was tested by comparing vehicle emissions results with those obtained from SUMO for Boston, Los Angeles, and Rio de Janeiro. The MODES equation accurately estimated emissions for 85%–87% of trips.

MODES is validated by direct CO_2 measurements of the Berkeley Air quality and CO2 Network ($BEACO_2N$). While both MODES and ($BEACO_2N$) estimates have various sources of uncertainties, they have comparable results for 9 km^2 spatial aggregation and 5 days of temporal aggregation. MODES estimates are lower than the $BEACO_2N$ estimates, mostly because of our use of average passanger vehicles with 25 mpg efficiency and lack of trucks (on average 7 mpg efficiency in the Bay Area) in our model.

Our mobility science informed emissions model is further evaluated against a hybrid model developed with highway vehicle counts, highway speeds and truck percentages acquired from PeMS highway sensors and emissions factors acquired from the CARB's EMFAC2017 model. Different than the validation with $BEACO_2N$ data, we used PEMS heavy duty vehicle percentage estimates in MODES. We assigned a percentage of the mobile phone travelers as trucks and assumed a 7 mpg efficiency for them. Comparisons of the hourly emission estimates on different highway segments showed that results of the two model's are within 35% of each other before and during the SIP orders.

The use of before and after COVID-19 SIP data is crucial for our validation. We show that the framework successfully captures the changes in mobility and associated emissions in the San Francisco Bay Area six weeks before and during the shelter-in-place order due to COVID-19. In our analysis, we show that the work-from-home behavior decreased the total number of weekday trips. However, the share of long-distance trips increased. Remote working improved the road conditions by lowering daily average network-wide congestion from 28% to 15%. The impact of the lowered congestion on vehicle efficiency is captured by the proposed framework. During the SIP, the median fuel efficiency of the trips increased by 6%–7% per vehicle type due to decreased congestion. Furthermore, we showed that on-road vehicle efficiency can vary by 70% from the manufacturer fuel economy depending on the vehicle speeds and stops.

Using individual mobility data allows us to relate emissions produced across the network to the home locations of travelers. This provides valuable insights into sustainable urban forms that local emission measurements cannot provide. We observe that cities with high population density have lower VKT and CO_2 emissions per person. Nevertheless, the congestion levels are higher for high population density regions. Considering the relationship obtained in Eq. (4), high population density is desirable from a climate change mitigation perspective. In Fig. 5A–B we also observe that less dense, peripheral cities have longer travel distances. For transportation decarbonization, it is key to not only shorten trips in dense cores but also tackle long commutes from peripheral areas.

Another advantage of the use of individual mobility data in the emissions estimates is the ability to quantify the disparities between the CO_2 production by different location sources. The ability to capture origin and destination pairs with the highest emissions has the potential to enrich policy interventions.

3.2. Policy implications

MODES offers actionable insights for multiple policy domains. First, it enables more effective environmental justice strategies by linking emissions to individual travel patterns and origins, allowing policymakers to identify both the communities generating emissions and those disproportionately exposed to them. This can support the design of socially equitable and targeted State Implementation Plans (SIPs), low-emission zones, and clean vehicle incentive programs. For example, in our work the residents of San Jose have the highest total emissions. Therefore, this region should be prioritized in mobility decarbonization efforts.

Second, MODES integrates smoothly into existing urban development and transportation project evaluation workflows. Since VKT and congestion are routinely computed in project assessments, MODES can directly estimate emissions impacts of alternative scenarios, aiding decisions about land-use changes, roadway expansions, and transit-oriented development (TOD). It also facilitates the assessment of policies such as congestion pricing—for an example combining distance- and time-based pricing seec (Zong, Zeng, & Li, 2024)- helping planners identify total emissions effects and distributional impacts.

Finally, MODES supports the evaluation of fuel economy policies while accounting for the rebound effect, where improved efficiency may lead to increased travel. By quantifying this effect, MODES helps policymakers design complementary strategies to ensure that fuel efficiency improvements translate into actual CO_2 reductions.

Taken together, the findings from MODES contribute to building urban mobility systems that are environmentally sustainable, socially equitable, and economically practical. By linking emissions to individual travel patterns and home locations, MODES offers critical insights for designing targeted interventions, particularly for addressing environmental justice concerns. Its reliance on widely available mobility and traffic data makes it suitable for rapid assessments of transportation and land-use scenarios, without the need for resource-intensive modeling. MODES thus serves as a practical decision-support tool for shaping urban environments that are cleaner and fairer.

3.3. Limitations

While MODES provides valuable insights, several limitations should be acknowledged. First, the model currently focuses on personal vehicles and does not fully account for heavy-duty vehicles due to data limitations. Second, the reliance on mobile phone data may underrepresent traveler groups without consistent device usage. Third, transit traffic (vehicles passing through the study region) is not explicitly modeled, which could affect estimates in high-throughput corridors. Fourth, MODES does not incorporate instantaneous acceleration profiles, which may cause some underestimation of emissions, particularly for highly dynamic driving patterns. Lastly, while CO_2 is well captured, criteria pollutants such as PM and NO_x require additional modeling steps to be integrated into the framework.

4. Future work

Future extensions of this work include incorporating heavy-duty vehicles, freight activity, and public transit into the emissions model, as well as improving demographic resolution to better capture equity considerations. We also plan to include trip purpose data and explicitly model through-traffic, which may affect high-flow corridors. The framework can be extended to support scenario analysis for evaluating the emissions impacts of specific policy interventions, such as vehicle electrification, congestion pricing, or low-emission zones. In addition, integrating urban metrics—such as land use diversity, shape indices, or sprawl indicators—into the analysis could provide insights into how urban form influences emission generation, strengthening the landscape-level analyses on local emissions in Li,

Table 1
Definitions of key terms and abbreviations.

Term/Abbreviation	Definition
CBG	Census Block Group, a geographical unit used in census data collection.
Congestion	Percentage deviation from the free-flow travel time on a road network (%).
Fuel Economy	Distance traveled per unit of fuel, measured in kilometers per liter (km/l) or miles per gallon (mpg).
SIP	Shelter-in-place orders.
VKT	Vehicle kilometers traveled (km).

Wang, Zhang, Zhu, and Yang (2024). Finally, incorporating dispersion modeling and expanding beyond CO_2 to include criteria pollutants like PM and NO_x would allow for a more complete assessment of transportation's environmental and public health impacts.

5. Conclusions

MODES provides a scalable, transferable, and data-efficient framework for estimating vehicular CO_2 emissions using individual-level mobility data. Its ability to relate emissions to VKT, congestion, and fleet fuel economy makes it suitable for rapid policy evaluation and scenario analysis. The model demonstrates good agreement with both bottom-up and top-down validation methods and offers practical insights into emissions patterns across different urban forms. Importantly, MODES highlights the potential for reducing per-capita emissions through VKT reduction strategies and identifies spatial disparities in emissions generation. This work contributes a valuable tool for transportation decarbonization and supports the design of equitable and effective climate and mobility policies.

6. Methods

6.1. Definitions

This section defines key terms used throughout the paper (see Table 1).

6.2. Individual mobility model

Mobile phone activity data and call detail records (CDR's) have been widely adopted in mobility modeling studies. In this work we utilized two datasets developed by mobile phone activity analysis: (1) TimeGeo urban mobility model (2) SafeGraph mobility data (SafeGraph, 2021).

The TimeGeo mobility model is a simulation framework designed to model urban travel demand by combining call detail records (CDRs) with individual mobility patterns. For this study, CDR data covering approximately 1.39 million users and over 200 million calls across the Bay Area over six weeks serve as the primary input. Each CDR entry includes anonymized user IDs, timestamps, call duration, and the geographic location of the connecting cell tower. The data is spatially refined to 892 distinct cell tower service areas, providing the granularity necessary to capture individual mobility choices. TimeGeo uses this data to simulate individual travel behavior by dividing each day into 144 discrete 10 min intervals and determining whether each individual remains at their current location or moves to another based on a probabilistic Markov chain model. The model's output is a simulated travel demand of approximately 13 million trips daily across 3.9 million individuals with known home locations (based on census tract data). Each trip is labeled with a purpose, aligning with typical urban mobility motifs, and the spatial and temporal distribution of trips aligns closely with observed urban commuting patterns. Further methodological details are presented in (Xu et al., 2018).

TimeGeo model in the San Francisco Bay Area built and validated against NHTS and CHTS (Xu et al., 2018) for a typical weekday. We adopted the trips in this model as the base scenario for the travel behavior before the shelter in place decisions. Each trip is associated with a user ID, home census tract for the user, trip purpose, timestamp and origin–destination coordinates.

To extend this model to the each day of the week for before and after shelter in place decisions we followed a simple scaling process using the SafeGraph data. We first extended the average weekday behavior before SIP to 5 days of the week. Then a daily-hourly flow change as a percentage between each OD is calculated.

SafeGraph, a data company that aggregates anonymized location data from numerous applications in order to provide insights about physical places, via the SafeGraph Community. To enhance privacy, SafeGraph excludes census block group information if fewer than five devices visited an establishment in a month from a given census block group (SafeGraph, 2021). Due to the aggregation steps towards meeting privacy requirements hourly origin–destination (OD) flows are not provided in any of the SafeGraph data products. We retrieved data from Neighborhood Patterns and Social Distancing Metrics between Jan 1–May 31, 2020. In our study area, SafeGraph data includes approximately 315,000 to 365,000 active devices per day, which corresponds to 4.4%–4.6% of the total population (7.95 million). To ensure representativeness, we normalized trip counts by the number of active devices and applied population-based scaling factors at the Census Block Group level. We inferred the hourly OD flows for each day of the week before and after shelter in place decisions combining these two datasets. Neighborhood Patterns data is one of the main products of the company which provides monthly analysis of census block group and point of interest visits. We used the *stops_by_each_hour* variable reporting the number of stops starting at each hour throughout the month for a CBG. Social Distancing Metrics product has been released following the COVID-19 confinements. For each origin CBG, destination CBG counts aggregated over a day is provided. We created the hourly OD matrix M as using the daily hourly origin–destination matrix D and the total hourly stops matrix S for each destination as following:

$$M_{i,j,t,d} = D_{i,j,d} S_{j,t,d} \quad (5)$$

where i's are origin CBGs, j's are destination CBGs, t is the hour of the day and d is the day of the month. The inferred daily hourly OD flows between CBGs are separated as before and after shelter in place flows. The OD flows then averaged for each weekday and hour pair to infer a representative behavior.

6.3. Road network and speeds

We obtain the San Francisco Bay Area road network as a directed graph where each edge is the road and each node is an intersection. Road and intersection geometry is acquired from Open Street Map (OSM). OSM provides road type, maximum speed and number of lanes associated with each road. For the intersections we retrieved traffic signals, stops, crossings, and junctions to model the stop and go traffic. To retain this information no simplification is performed on the final graph.

The hourly speed values are retrieved from the Uber Movement Speeds API which provides hourly mean speed values of the street segments in several metropolitan areas starting from 2018. In this project, the data between 06/2019 and 4/2020 is retrieved. Its important to note that, Uber Movement API stopped reporting data after 4/2020. Due to Uber's data collection and reporting protocol, we do not have hourly speed values on all of the streets. Only the road segments that attracted enough traffic in each hour are included to protect customer privacy. Therefore to get the missing speed values, we applied a K-nearest neighbors (KNN) data imputation method to have a network with complete information. (see Supplementary Notes S1)

Uber Movement Speeds values are based on averaged and anonymized GPS data from Uber's ride-hailing vehicles, which generally follow typical traffic patterns, though they may not capture all aspects of general vehicle flow.

6.4. Fuel consumption and vehicle emissions model

Fuel consumption of the trips is estimated with the regression based model StreetSmart. This model is developed using the OBD-II and GPS data collected from 600 miles of driving. Authors included 4 variables in the final model after testing a range of parameters. The final model with a mean accuracy of 96% in the tested scenarios is presented in Eq. (1).

The model predicts the fuel consumption in US gallons. T_{idle} is the stopping time, T_{move} is the moving time in seconds, a is acceleration in $\frac{\text{m}}{\text{s}^2}$ integrated over the distance and L is the distance driven in km. The k's in the model are vehicle efficiency specific constants and they are calibrated for different vehicle efficiency bins. The model presented is detailed enough to capture the efficiency changes due to the speed variations and stop-and-go traffic. We further validated this model with Autonomie simulations and EPA speed profiles. The results are presented in Fig. 2.

We converted the gallons of fuel consumption to CO_2 emissions in grams using the CO_2 intensity of the fuel. We take the fuel density as $0.75\ \frac{\text{g}}{\text{ml}}$ and carbon intensity of the fuel by weight as $0.86\frac{gC}{gFuel}$. Carbon is converted into carbon dioxide in the combustion process with a weight ratio of 12 to 44.

6.5. CO_2 sensor measurements

We use hourly CO_2 observations from the Berkeley Air quality and CO_2 Network ($BEACO_2N$). The CO_2 observations are converted to hourly emissions with Stochastic-Time Inverted Lagrangian Transport (STILT) model, coupled with a Bayesian inversion (Turner, Kim et al., 2020).

The inversion process requires meteorology data and prior emission estimates from different sources. Prior emissions sources included in the $BEACO_2N - STILT$ inversion are home heating data distributed spatially according to population density, fuel sales data distributed spatially according to vehicle counts (McDonald et al., 2014) and biogenic inventory derived using Solar Induced Fluorescence (SIF) satellite data (Turner, Köhler et al., 2020). The resulting posterior emissions are stored in $1\ \text{km}^2$ grid cells. Transportation emissions are estimated by subtracting the non-transportation priori sources from posterior emissions. $BEACO_2N - STILT$ inversion is estimated to be precise to at least 30% for a line source (Turner et al., 2016).

The influence region of the sensors are the regions that the emissions are likely to be originated from. In this work we followed Fitzmaurice et al. (2022) and included the 40% influence region in the analysis.

CRediT authorship contribution statement

Ayşe Tuğba Öztürk: Writing – review & editing, Writing – original draft, Visualization, Validation, Software, Methodology, Formal analysis, Data curation, Conceptualization. **Aparimit Kasliwal:** Data curation. **Helen Fitzmaurice:** Writing – review & editing, Validation, Methodology, Data curation. **Olga Kavvada:** Writing – review & editing, Supervision, Project administration, Methodology. **Philippe Calvez:** Supervision, Project administration. **Ronald C. Cohen:** Validation, Supervision, Methodology. **Marta C. González:** Writing – review & editing, Supervision, Project administration, Methodology, Investigation, Funding acquisition, Conceptualization.

Declaration of competing interest

The authors declare that they have no known competing financial interests or personal relationships that could have appeared to influence the work reported in this paper.

Acknowledgments

This work was supported by Engie SA, the ITS-SB1 Berkeley Statewide Transportation Research Program and the California Air Resources Board.

Appendix A. Supplementary data

Supplementary material related to this article can be found online at https://doi.org/10.1016/j.scs.2025.106421.

Data availability

Data will be made available on request.

References

Abou-Senna, H., Radwan, E., Westerlund, K., & Cooper, C. D. (2013). Using a traffic simulation model (VISSIM) with an emissions model (MOVES) to predict emissions from vehicles on a limited-access highway. *Journal of the Air & Waste Management Association*, *63*(7), 819–831. http://dx.doi.org/10.1080/10962247.2013.795918.

Anya, A. R., Rouphail, N. M., Frey, H. C., & Schroeder, B. (2014). Application of AIMSUN microsimulation model to estimate emissions on signalized arterial corridors. *Transportation Research Record*, *2428*(1), 75–86. http://dx.doi.org/10.3141/2428-09.

Arcaute, E., Hatna, E., Ferguson, P., Youn, H., Johansson, A., & Batty, M. (2015). Constructing cities, deconstructing scaling laws. *Journal of the Royal Society Interface*, *12*(102), Article 20140745. http://dx.doi.org/10.1098/rsif.2014.0745.

Bandeira, J. M., Coelho, M. C., Sá, M. E., Tavares, R., & Borrego, C. (2011). Impact of land use on urban mobility patterns, emissions and air quality in a portuguese medium-sized city. *Science of the Total Environment*, *409*(6), 1154–1163. http://dx.doi.org/10.1016/j.scitotenv.2010.12.008.

Banister, D. (2011). Cities, mobility and climate change. *Journal of Transport Geography*, *19*(6), 1538–1546.

Barthelemy, M. (2019a). The statistical physics of cities. *Nature Reviews Physics*, *1*(6), 406–415.

Barthelemy, M. (2019b). Tomography of scaling. *Journal of the Royal Society Interface*, *16*(160), Article 20190602.

Bettencourt, L. M. A. (2013). The origins of scaling in cities.. *Science*, *340*(6139), 1438–1441.

Bettencourt, L. M. A., Lobo, J., Helbing, D., Kühnert, C., & West, G. B. (2007). Growth, innovation, scaling, and the pace of life in cities. *Proceedings of the National Academy of Sciences of the United States of America*, *104*(17), 7301–7306.

Bettencourt, L. M. A., Samaniego, H., & Youn, H. (2014). Professional diversity and the productivity of cities.. *Scientific Reports*, *4*, 5393.

Blaudin de Thé, C., Carantino, B., & Lafourcade, M. (2020). The carbon 'carprint' of suburbanization: New evidence from french cities. Retrieved from https://halshs.archives-ouvertes.fr/halshs-02572893 (Working paper or preprint, PSE Working Papers n°2020-26).

Böhm, M., Nanni, M., & Pappalardo, L. (2022). Gross polluters and vehicle emissions reduction. *Nature Sustainability*, *5*(160), 699–707.

Bureau of Transportation Statistics (2022). Trips by distance band. In *Bureau of transportation statistic*: *Tech. Rep.*, Bureau of Transportation Statistics, https://www.bts.gov/browse-statistical-products-and-data/covid-related/trips-distance-groupings-national-or-state. [Accessed 10 January 2022].

California Air Resources Board (2017). *EMFAC2017 - emission factors model technical documentation*: *Tech. Rep.*, California Air Resources Board, Retrieved from https://ww2.arb.ca.gov/our-work/programs/emfac2017.

California Air Resources Board (2018). *2018 PROGRESS REPORT: California's sustainable communities and climate protection act*: *Tech. Rep.*, California Air Resources Board, Retrieved from https://ww2.arb.ca.gov/legislatively-mandated-reports, Legislatively Mandated Reports, [Accessed 10 January 2022].

Caltrans performance measurement system. (2021). Retrieved from https://pems.dot.ca.gov/. [Accessed 28 January 2022].

Caubel, J. J., Cados, T. E., Preble, C. V., & Kirchstetter, T. W. (2019). A distributed network of 100 black carbon sensors for 100 days of air quality monitoring in west Oakland, California. *Environmental Science and Technology*, *53*(13), 7564–7573. http://dx.doi.org/10.1021/acs.est.9b00282.

Çolak, S., Lima, A., & González, M. C. (2016). Understanding congested travel in urban areas. *Nature Communications*, *7*(1), 10793.

Cottineau, C., Hatna, E., Arcaute, E., & Batty, M. (2017). Diverse cities or the systematic paradox of urban scaling laws. *Computers, Environment and Urban Systems*, *63*, 80–94.

Depersin, J., & Barthelemy, M. (2018). From global scaling to the dynamics of individual cities. *Proceedings of the National Academy of Sciences*, *115*, 2317–2322, 10.

(EPA), U. E. P. A. (2021). *Federal test procedure*: *Tech. Rep.*, U.S. Environmental Protection Agency (EPA).

European Environment Agency (2020). *Trends and projections in Europe 2021: Tracking progress towards Europe's climate and energy targets*: *Tech. Rep.*, European Environment Agency.

Faris, W. F., Rakha, H. A., Kafafy, R. I., Idres, M., & Elmoselhy, S. (2011). Vehicle fuel consumption and emission modelling: An in-depth literature review. *International Journal of Vehicle Systems Modelling and Testing*, *6*(3/4), 318. http://dx.doi.org/10.1504/IJVSMT.2011.04423.

Fitzmaurice, H. L., Turner, A. J., Kim, J., Chan, K., Delaria, E. R., Newman, C., et al. (2022). Assessing vehicle fuel efficiency using a dense network of CO_2 observations. *Atmospheric Chemistry and Physics*, *22*(6), 3891–3900.

Fontes, T., Pereira, S. R., Fernandes, P., Bandeira, J. M., & Coelho, M. C. (2015). How to combine different microsimulation tools to assess the environmental impacts of road traffic? Lessons and directions. *Transportation Research Part D: Transport and Environment*, *34*, 293–306. http://dx.doi.org/10.1016/j.trd.2014.11.023.

Fragkias, M., Lobo, J., Strumsky, D., & Seto, K. C. (2013). Does size matter? Scaling of CO2 emissions and U.S. urban areas. *PLoS One*, *8*(6), 1–8. http://dx.doi.org/10.1371/journal.pone.0064727.

Gately, C. K., & Hutyra, L. R. (2017). Large uncertainties in urban-scale carbon emissions. *Journal of Geophysical Research: Atmospheres*, *122*(20), 11–242.

Gately, C. K., Hutyra, L. R., Peterson, S., & Sue Wing, I. (2017). Urban emissions hotspots: Quantifying vehicle congestion and air pollution using mobile phone GPS data. *Environmental Pollution*, *229*, 496–504. http://dx.doi.org/10.1016/j.envpol.2017.05.091.

Gately, C. K., Hutyra, L. R., & Wing, I. S. (2015). Cities, traffic, and CO2: A multidecadal assessment of trends, drivers, and scaling relationships. *Proceedings of the National Academy of Sciences*, *112*(16), 4999–5004. http://dx.doi.org/10.1073/pnas.1421723112.

Gurney, K. R., Liang, J., Roest, G., Song, Y., Mueller, K., & Lauvaux, T. (2021). Underreporting of greenhouse gas emissions in U.S. cities. *Nature Communications*, *12*(1), 553,

Gurney, K. R., Mendoza, D. L., Zhou, Y., Fischer, M. L., Miller, C. C., Geethakumar, S., et al. (2009). High resolution fossil fuel combustion CO2 emission fluxes for the United States. *Environmental Science and Technology*, *43*(14), 5535–5541. http://dx.doi.org/10.1021/es900806c.

Gurney, K., Razlivanov, I., Song, Y., Zhou, Y., Benes, B., & Abdul-Massih, M. (2012). Quantification of fossil fuel CO2 emissions on the building/street scale for a large U.S. city. *Environmental Science and Technology*, *46*(21), 12194–12202.

International Council on Clean Transportation (2024). *Cleaning up Germany's vehicle stock: Strategies to decarbonize the passenger car fleet*: *Tech. Rep.*, International Council on Clean Transportation.

Jiang, S., Yang, Y., Gupta, S., Veneziano, D., Athavale, S., & González, M. C. (2016). The TimeGeo modeling framework for urban mobility without travel surveys. *Proceedings of the National Academy of Sciences*, *113*(37), E5370–E5378. http://dx.doi.org/10.1073/pnas.1524261113, arXiv:https://www.pnas.org/content/113/37/E5370.full.pdf.

Kalila, A., Awwad, Z., Di Clemente, R., & González, M. C. (2018). Big data fusion to estimate urban fuel consumption: A case study of riyadh. *Transportation Research Record*, *2672*(24), 49–59. http://dx.doi.org/10.1177/0361198118798461.

Kwon, J., Varaiya, P., & Skabardonis, A. (2003). Estimation of truck traffic volume from single loop detectors with lane-to-lane speed correlation. *Transportation Research Record*, *1856*(1), 106–117. http://dx.doi.org/10.3141/1856-11.

Lauvaux, T., Miles, N. L., Deng, A., Richardson, S. J., Cambaliza, M. O., Davis, K. J., et al. (2016). High-resolution atmospheric inversion of urban CO2 emissions during the dormant season of the Indianapolis flux experiment (INFLUX). *Journal of Geophysical Research: Atmospheres*, *121*(10), 5213–5236. http://dx.doi.org/10.1002/2015JD024473.

Li, S., Wang, J., Zhang, Y., Zhu, C., & Yang, J. (2024). Spatiotemporal patterns and the influence mechanism of urban landscape pattern on carbon emission performance: Evidence from Chinese cities. *Sustainable Cities and Society*, *102*, Article 105644. http://dx.doi.org/10.1016/j.scs.2023.105644.

Louf, R., & Barthelemy, M. (2014a). How congestion shapes cities: From mobility patterns to scaling. *Scientific Reports*, *4*(1), 1–9.

Louf, R., & Barthelemy, M. (2014b). Scaling: Lost in the smog. *Environment and Planning B: Planning and Design*, *41*(5), 767–769. http://dx.doi.org/10.1068/b4105c.

McDonald, B. C., McBride, Z. C., Martin, E. W., & Harley, R. A. (2014). High-resolution mapping of motor vehicle carbon dioxide emissions. *Journal of Geophysical Research: Atmospheres*, *119*(9), 5283–5298. http://dx.doi.org/10.1002/2013JD021219.

Miller, E. J., & Ibrahim, A. (1998). Urban form and vehicular travel: Some empirical findings. *Transportation Research Record*, *1617*(1), 18–27. http://dx.doi.org/10.3141/1617-03.

Milojevic-Dupont, N., & Creutzig, F. (2020). Machine learning for geographically differentiated climate change mitigation in urban areas. *Sustainable Cities and Society*, *60*, Article 102213. http://dx.doi.org/10.1016/j.scs.2020.102213.

Mohajeri, N., Gudmundsson, A., & French, J. R. (2015). CO2 emissions in relation to street-network configuration and city size. *Transportation Research Part D: Transport and Environment*, *35*, 116–129. http://dx.doi.org/10.1016/j.trd.2014.11.025.

Newman, M. E. J. (2005). Power laws, Pareto distributions and Zipf's law. *Contemporary Physics*, *46*(5), 323–351.

Ntziachristos, L., Gkatzoflias, D., Kouridis, C., & Samaras, Z. (2009). COPERT: A European road transport emission inventory model. In *Information technologies in environmental engineering*. Retrieved from https://api.semanticscholar.org/CorpusID:36346162.

Nyhan, M., Sobolevsky, S., Kang, C., Robinson, P., Corti, A., Szell, M., et al. (2016). Predicting vehicular emissions in high spatial resolution using pervasively measured transportation data and microscopic emissions model. *Atmospheric Environment*, *140*, 352–363.

Oehlerking, A. L. (2011). *streetSmart : modeling vehicle fuel consumption with mobile phone sensor data through a participatory sensing framework* [Ph.D. thesis], Massachusetts Institute of Technology, Department of Mechanical Engineering.

Olmos, L. E., Çolak, S., Shafiei, S., Saberi, M., & González, M. C. (2018). Macroscopic dynamics and the collapse of urban traffic. *Proceedings of the National Academy of Sciences of the United States of America*, *115*(50), 12654–12661.

Panis, L. I., Broekx, S., & Liu, R. (2006). Modelling instantaneous traffic emission and the influence of traffic speed limits. *Science of the Total Environment*, *371*(1–3), 270–285. http://dx.doi.org/10.1016/j.scitotenv.2006.08.017.

Pappalardo, L., Manley, E., Sekara, V., & Alessandretti, L. (2023). Future directions in human mobility science. *Nature Computational Science*, *3*(7), 588–600.

Patankar, N., Lin, J., & Patankar, T. (2021). Mileage efficiency of cars. *Cleaner Engineering and Technology*, *4*, Article 100240. http://dx.doi.org/10.1016/j.clet.2021.100240.

Peters, G., Andrew, R., Canadell, J., Friedlingstein, P., Jackson, R., Korsbakken, J., et al. (2019). Carbon dioxide emissions continue to grow despite emerging climate policies. *Nature Climate Change*, *10*.

Ramaswami, A., Tong, K., Canadell, J. G., Jackson, R. B., Stokes, E. K., Dhakal, S., et al. (2021). Carbon analytics for net-zero emissions sustainable cities. *Nature Sustainability*, *4*(6), 460–463. http://dx.doi.org/10.1038/s41893-021-00715-5.

SafeGraph. (2021). Retrieved from https://www.safegraph.com. [Accessed 01 March 2021].

Shusterman, A. A., Teige, V. E., Turner, A. J., Newman, C., Kim, J., & Cohen, R. C. (2016). The berkeley atmospheric CO_2 observation network: initial evaluation. *Atmospheric Chemistry and Physics*, *16*(21), 13449–13463. http://dx.doi.org/10.5194/acp-16-13449-2016.

Smit, R., Ntziachristos, L., & Boulter, P. (2010). Validation of road vehicle and traffic emission models–a review and meta-analysis. *Atmospheric Environment*, *44*(25), 2943–2953.

Turner, A. J., Kim, J., Fitzmaurice, H., Newman, C., Worthington, K., Chan, K., et al. (2020). Observed impacts of COVID-19 on urban CO2 emissions. *Geophysical Research Letters*, *47*(22), Article e2020GL090037. http://dx.doi.org/10.1029/2020GL090037.

Turner, A. J., Köhler, P., Magney, T. S., Frankenberg, C., Fung, I., & Cohen, R. C. (2020). A double peak in the seasonality of California's photosynthesis as observed from space. *Biogeosciences*, *17*(2), 405–422. http://dx.doi.org/10.5194/bg-17-405-2020.

Turner, A. J., Shusterman, A. A., McDonald, B. C., Teige, V., Harley, R. A., & Cohen, R. C. (2016). Network design for quantifying urban CO_2 emissions: Assessing trade-offs between precision and network density. *Atmospheric Chemistry and Physics*, *16*(21), 13465–13475. http://dx.doi.org/10.5194/acp-16-13465-2016.

Uber movement. (2021). Retrieved from https://movement.uber.com/?lang=en-US. [Accessed 01 May 2021].

United States Environmental Protection Agency (USEPA) (2023). *Motor Vehicle Emission Simulator: MOVES4*: *Tech. Rep.*, United States Environmental Protection Agency, Retrieved from https://www.epa.gov/moves. (Version 4.0.0).

U. S. Department of Energy (2021). *Fuel economy guide: model year 2021*: *Tech. Rep.*, U.S. Department of Energy, Last checked: May 2021.

U. S. Environmental Protection Agency (EPA) (2018). *Greenhouse gas emissions from a typical passenger vehicle*: *Tech. Rep.*, U.S. Environmental Protection Agency.

U. S. Environmental Protection Agency (EPA) (2019). *Inventory of US greenhouse gas emissions and sinks: 1990–2017*: *Tech. Rep.*, U.S. Environmental Protection Agency.

Wu, X., Yang, D., Wu, R., Gu, J., Wen, Y., Zhang, S., et al. (2022). High-resolution mapping of regional traffic emissions using land-use machine learning models. *Atmospheric Chemistry and Physics*, *22*, 1939–1950. http://dx.doi.org/10.5194/acp-22-1939-2022.

Xu, Y., Çolak, S., Kara, E. C., Moura, S. J., & González, M. C. (2018). Planning for electric vehicle needs by coupling charging profiles with urban mobility. *Nature Energy*, *3*(6), 484–493.

Xu, Y., Olmos, L. E., Abbar, S., & González, M. C. (2020). Deconstructing laws of accessibility and facility distribution in cities. *Science Advances*, *6*(37), eabb4112.

Yao, J., & Moawad, A. (2019). Vehicle energy consumption estimation using large scale simulations and machine learning methods. *Transportation Research Part C: Emerging Technologies*, *101*, 276–296. http://dx.doi.org/10.1016/j.trc.2019.02.012.

Yigitcanlar, T., Kamruzzaman, M., Foth, M., Sabatini-Marques, J., da Costa, E., & Ioppolo, G. (2019). Can cities become smart without being sustainable? A systematic review of the literature. *Sustainable Cities and Society*, *45*, 348–365. http://dx.doi.org/10.1016/j.scs.2018.10.009.

Zhang, S. J., Niu, T. L., Wu, Y., Zhang, K. M., Wallington, T. J., Xie, Q. Y., et al. (2018). Fine-grained vehicle emission management using intelligent transportation system data. *Environmental Pollution*, *241*, 1027–1037. http://dx.doi.org/10.1016/j.envpol.2018.06.003.

Zong, F., Zeng, M., & Li, Y.-X. (2024). Congestion pricing for sustainable urban transportation systems considering carbon emissions and travel habits. *Sustainable Cities and Society*, *105198*, http://dx.doi.org/10.1016/j.scs.2024.105198.